THE JOURNAL OF PHYSICAL CHEMISTRY C
A JOURNAL OF THE AMERICAN CHEMICAL SOCIETY

pubs.acs.org/JPCC Article

Molecular Charge Transfer Effects on Perylene Diimide Acceptor and Dinaphthothienothiophene Donor Systems

Nadine Rußegger,* Ana M. Valencia, Lena Merten, Matthias Zwadlo, Giuliano Duva, Linus Pithan, Alexander Gerlach, Alexander Hinderhofer, Caterina Cocchi, and Frank Schreiber

Cite This: *J. Phys. Chem. C* 2022, 126, 4188−4198 Read Online

ACCESS | Metrics & More | Article Recommendations | Supporting Information

ABSTRACT: The interactions between organic donor and acceptor molecules and the related charge transfer (CT) effects are of great interest in organic optoelectronics. Here, we present a comprehensive investigation of cocrystal formation and charge transfer effects in weakly interacting organic semiconductor mixtures. As a model system, we choose dinaphthothienothiophene (DNTT) as a donor molecule and two different perylene diimide derivatives (PTCDI-C_8-CN_2 and PDIF-CN_2) as acceptors, which differ in the fluorination of the side chains in the imide position. Experimentally, both systems show a small ground-state CT governed by hybridized HOMO−1 and LUMO+1 levels. In contrast, the respective HOMO and LUMO levels of the complex are localized on the acceptor and donor molecule. This leads to the observation of a nearly pure charge transfer excitation from the acceptor to the donor in the absorption spectra. We discuss the general impact of localized HOMO and LUMO levels on the optoelectronic properties in CT complexes dependent on comparison with first-principles calculations based on density functional theory and many-body perturbation theory.

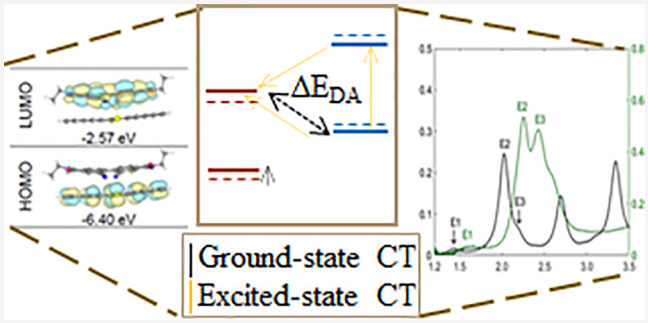

■ INTRODUCTION

Organic optoelectronic devices such as organic photovoltaic cells and organic light-emitting diodes are an attractive alternative to their inorganic counterparts. One of the fundamental processes in such devices relies on molecular charge transfer (CT) which takes place at the interface of donor and acceptor molecules, for example, in molecular mixed crystals.[1,2] The microscopic details of CT, in particular for the different strengths of interactions, are still not fully understood. In a rather common approach, molecular charge transfer can be roughly divided into several cases depending on how much the molecules interact with each other. For weakly bound organic molecules a partial charge transfer on average from the donor to the acceptor is expected.[3−5] In this context, the morphology and intermixing on the molecular level in bulk heterojunction thin films have a great impact.[6−10]

One group of organic small molecules that are widely used as electron donors and acceptors in electronic devices, especially for organic field effect transistors, are perylene diimide (PDI) derivatives.[11,12] They are very promising n-type organic materials due to their relatively strong electron affinities. Their charge-transport properties can be tailored upon changing the substituents on the imide or the bay position of the perylene backbone.[11−14] It was shown that alkyl, branched, and fluorinated side chains and electron-withdrawing side groups can alter molecular packing and morphology of the deposited thin films.[15−17] These materials are structurally well-defined and can therefore serve as an acceptor model system. There is only a few reports related to donor−acceptor thin films with PDI derivatives.[18−20]

In this paper, we present a comprehensive experimental and first-principles study on charge transfer effects and cocrystal formation in weakly interacting organic small molecule donor−acceptor systems. We focus on ground-state (GS-CT) and excited-state (ES-CT) charge transfer effects in these thin film systems and discuss fundamental characteristics because a complete understanding of the CT mechanism for this type of systems has not been achieved. As a model system, we choose dinaphthothienothiophene (DNTT) as donor and two different perylene diimide derivatives (PTCDI-C_8-CN_2 and PDIF-CN_2) as acceptors, which differ in the fluorination of the side chains in the imide position. Because of its known applications in organic electronics, DNTT is used as a donor because the molecule matches perfectly with its structure and its energy levels allow for a CT effect with the different perylene diimide

Received: December 3, 2021
Revised: February 8, 2022
Published: February 18, 2022

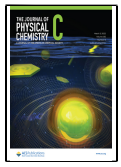

https://doi.org/10.1021/acs.jpcc.1c10281
J. Phys. Chem. C 2022, 126, 4188−4198

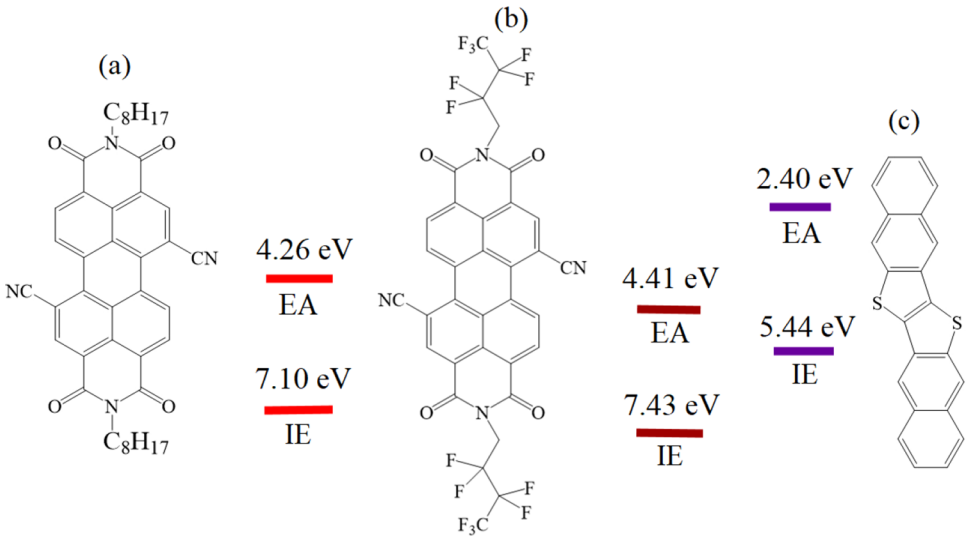

Figure 1. Overview of the studied perylene diimide acceptor molecules with the different electron affinities (EA) and ionization energies (IE). The IEs levels are determined by ultraviolet photoelectron spectroscopy of the thin films,[5,21,31] and the EAs are calculated with the IEs, the optical band gaps, and the exciton binding energies: (a) PTCDI-C_8-CN_2, (b) PDIF-CN_2, and (c) donor molecule DNTT.

derivatives.[21−23] We discuss the different mixing behavior for the two studied DNTT:PDI thin film systems by grazing-incidence wide-angle X-ray scattering (GIWAXS) combined with optical spectroscopy for excited-state (absorption and emission) and ground-state CT effects (infrared spectroscopy). It was already shown that PDIF-CN_2 as well as another PDI derivative (PDIR-CN_2) can form a well-defined cocrystal and partial charge transfer effects with the donor molecule diindenoperylene (DIP).[5,24] We correlate optical spectroscopy, structural characterization, and first-principles calculations to investigate the impact of the side chain on perylene diimide:DNTT cocrystalline thin films.

■ METHODS

Experimental Details. DNTT is purchased from Sigma-Aldrich (purity of 98%); PTCDI-C_8-CN_2 and PDIF-CN_2 are from Flexterra and used as received (see Figure 1). The thin films are prepared by organic molecular beam deposition (OMBD) under ultrahigh vacuum ($p \approx 2 \times 10^{-10}$ mbar).[25,26] Three different substrates are used for the different structural and optical investigations: a silicon 111 wafer with a native oxide layer of 2 nm (for X-ray reflectivity (XRR), GIWAXS, infrared, and photoluminescence measurements), a glass wafer which is roughened at the backside, and a transparent glass wafer (for UV/vis/NIR spectroscopy). The substrates are cleaned with acetone and isopropyl alcohol in an ultrasonic bath each for 10 min and degassed overnight in the chamber before film preparation. The substrates are kept at constant temperature of 293 or 423 K, respectively, during film growth. Mixed thin films are prepared by coevaporation[6] of the donor molecule DNTT and the different perylene diimide derivatives with a mixing ratio of 2:1, 1:1, and 1:2. The nominal thicknesses of about 20 nm and growth rates of about 0.2 nm min^{-1} in total are controlled by a quartz crystal microbalance (QCM) during film growth and calibrated by X-ray reflectivity.

For structural analysis, XRR is measured with a GE Inspection Technologies XRD 3003 TT system using Cu $K\alpha_1$ radiation (λ = 1.5406 Å). XRR data fitting is done with GenX[27] by means of the Parratt formalism.[28] GIWAXS measurements are performed at the beamline P03 of DESY (Hamburg, Germany)[29] and at the beamline ID03 of ESRF (Grenoble, France) by using a focused beam with a wavelength of 0.9686 and 0.992 Å. UV/vis/NIR spectra are acquired by using a Varian Cary 50 spectrometer in the wavelength range of 200−1100 nm at normal incidence. Photoluminescence spectra are obtained by using a Horiba Jobin Yvon Labram HR 800 spectrometer with a CCD 1024 × 256 detector. For PL excitation a Nd:YAG laser with a wavelength of 532 nm is used. Temperature-dependent PL spectra are determined with a cooling CryoVac system with liquid nitrogen in the range from 293 to 77 K.[30] Infrared spectra are acquired by using a Vertex 70 FTIR spectrometer (Bruker) in transmission mode.

Theoretical Methods and Computational Details. Ground- and excited-state properties of the systems considered in this work are computed from density functional theory (DFT)[32,33] and many-body perturbation theory (MBPT),[34] including the single-shot G_0W_0 approximation[35] and the solution of the Bethe−Salpeter equation (BSE).[36] Equilibrium geometries of the individual donor and acceptor molecules as well as of the complexes are computed with the all-electron code FHI-aims,[37] adopting tight integration grids and TIER2 basis sets.[38] The generalized-gradient approximation for the exchange-correlation potential is adopted in the Perdew−Burke−Ernzerhof[39] parametrization. The van der Waals interactions are accounted for by the Tkatchenko−Scheffler scheme.[40] Atomic positions are relaxed until the Hellmann−Feynman forces are smaller than 10^3 eV/Å. From these calculations we estimate the charge transfer using the Hirshfeld partition scheme.[41]

The MOLGW code[42] is employed to compute the electronic and optical properties of all systems. Gaussian-type cc-pVDZ basis sets[43] are adopted including the frozen-core approximation. The resolution-of-identity approximation is also employed.[44] The hybrid functional PBE0[45] is used to provide an enhanced starting point for the G_0W_0 calculations in the considered π-conjugated molecules.[46,47] The BSE is solved in the Tamm−Dancoff approximation[48] including in the transition space all the occupied and unoccupied states available from the basis set. To evaluate the character and

https://doi.org/10.1021/acs.jpcc.1c10281
J. Phys. Chem. C 2022, 126, 4188−4198

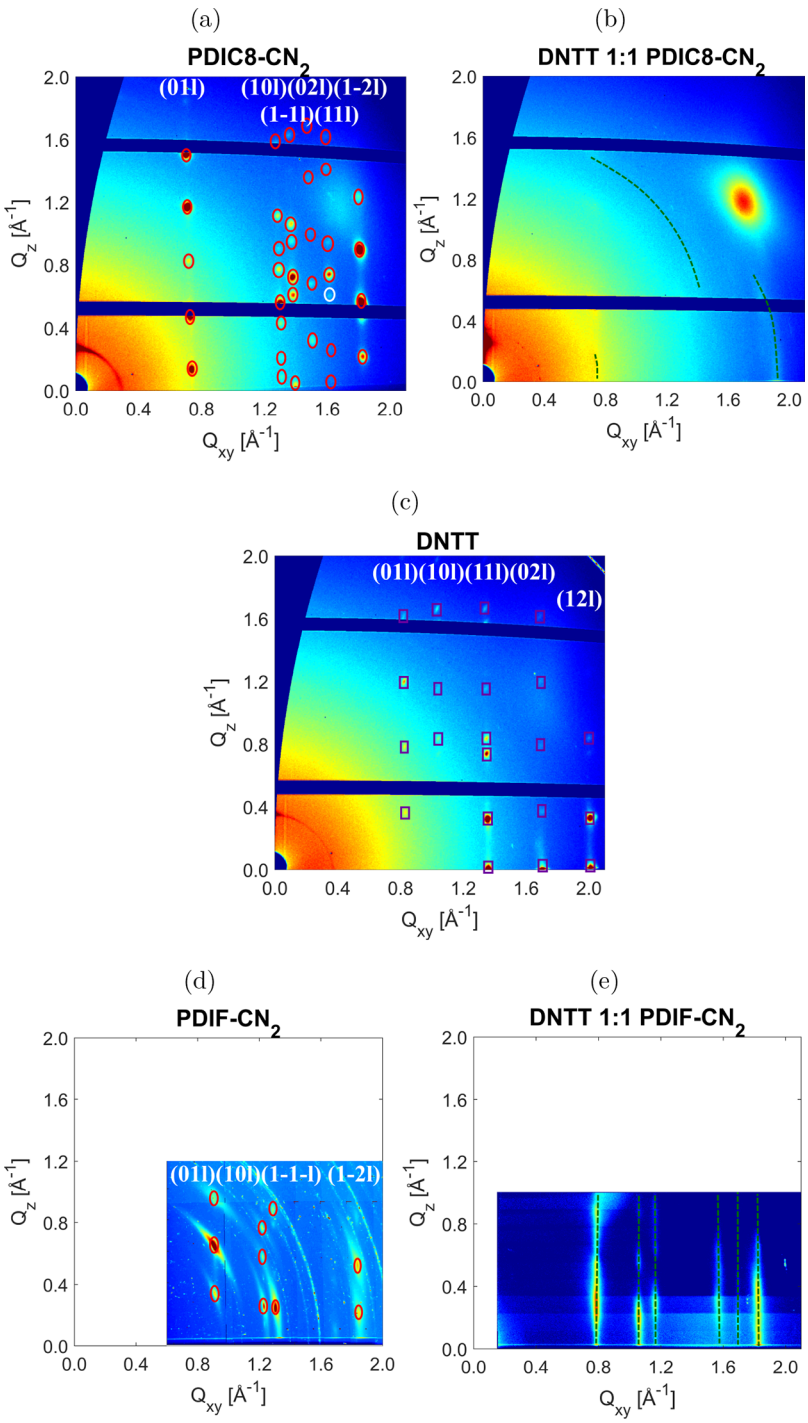

Figure 2. GIWAXS data of (a) PDIC$_8$-CN$_2$ (150 °C), (b) DNTT 1:1 PDIC$_8$-CN$_2$ (25 °C), (c) DNTT (100 °C), (d) PDIF-CN$_2$ (140 °C), and (e) DNTT 1:1 PDIF-CN$_2$ (150 °C) (squares indicate peaks of the donor, circles of the acceptor, and dashed green lines for the mixed phase; the same q-ranges were taken for clarity).

the spatial distribution of the excitons, we compute the hole and electron density,[49,50] which defined the λth excitation as

$$\rho_h^\lambda(\mathbf{r}) = \sum_{\alpha\beta} A_{\alpha\beta}^\lambda |\phi_\alpha(\mathbf{r})|^2 \tag{1}$$

and

$$\rho_e^\lambda(\mathbf{r}) = \sum_{\alpha\beta} A_{\alpha\beta}^\lambda |\phi_\beta(\mathbf{r})|^2 \tag{2}$$

respectively. The coefficients $A_{\alpha\beta}^\lambda$ are the square of the normalized BSE eigenvectors and weight each transition between occupied (ϕ_α) and unoccupied (ϕ_β) states.

RESULTS AND DISCUSSION

Structural Characterization. First, we discuss the structure of mixed DNTT:PDI thin films depending on the different side chain in the imide position of the acceptor molecules. An overview of the measured GIWAXS diffraction patterns from both pure perylene diimide derivatives and the

https://doi.org/10.1021/acs.jpcc.1c10281
J. Phys. Chem. C 2022, 126, 4188−4198

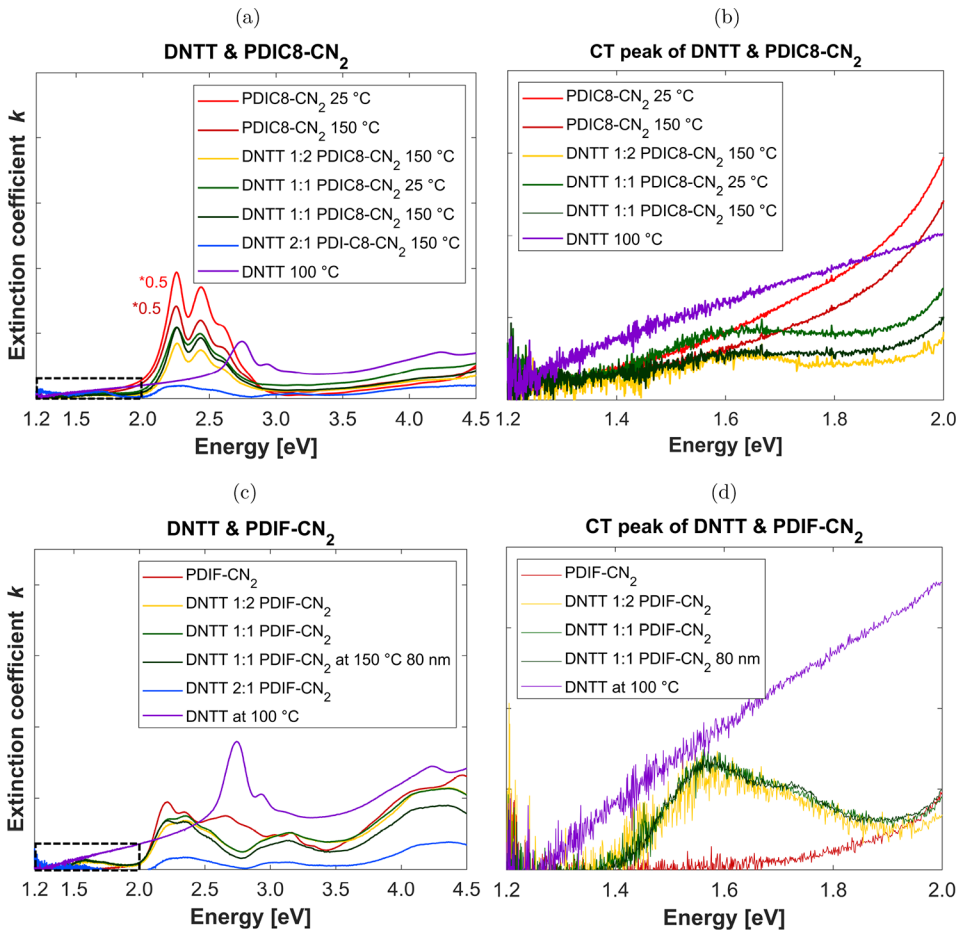

Figure 3. Absorption spectra of (a) DNTT and $PDIC_8$-CN_2 mixed films deposited at 25 and 150 °C, (b) enlarged section of the CT peak (black marked area of part a), (c) DNTT and PDIF-CN_2 mixed films deposited at 150 °C, and (d) enlarged section of the CT peak (black marked area of part c). The spectra are scaled for clarity.

donor molecule DNTT as well as the equimolar donor–acceptor mixtures is shown in Figure 2.

All three pure compounds form crystalline thin films with Bragg reflections belonging to known crystal structures (Figure 2a,c,d).[51−53] All molecules are oriented with their longest axis almost normal to the substrate surface. The tilt angles of the respective molecules to the silicon substrate are 68.11° for PTCDI-C_8-CN_2 ($PDIC_8$-CN_2), 85.47° for DNTT, and 73.92° for PDIF-CN_2 assuming the known crystal structures. The crystal quality of the acceptors depends strongly on the substrate temperature during deposition. In thin films PDIF-CN_2 is only crystalline on SiO_2 (and not on the other substrates employed) at a deposition temperature higher than 120 °C in contrast to $PDIC_8$-CN_2, which forms crystalline films already at room temperature.[54]

Figures 2b and 2e show GIWAXS data of the equimolar DNTT:$PDIC_8$-CN_2 and DNTT:PDIF-CN_2 mixed films. In both reciprocal space maps only signals from the mixed cocrystals are visible (marked by dashed green lines). The donor DNTT has roughly the size of the PDI core and exhibits different mixing behavior with the two acceptor compounds.

$PDIC_8$-CN_2 forms a cocrystal with DNTT when codeposited at room temperature; however, it tends to phase-separate at higher substrate temperatures. Figure 2b shows GIWAXS data of a $PDIC_8$-CN_2:DNTT 1:1 mixed film deposited at 25 °C. The weak ring-shaped features indicate the formation of 1:1 cocrystalline grains without preferred orientation. Signals of the pure $PDIC_8$-CN_2 are visible for both equimolar thin films in the X-ray reflectivity scans (see Figure S1), showing that at higher substrate temperature phase-separating into the pure compounds occurs. In contrast, the donor DNTT and the acceptor PDIF-CN_2 form a well-defined highly ordered cocrystal visible in the GIWAXS data in Figure 2e. In the reciprocal space maps and in the XRR spectra (see Figure S2) of the equimolar and the PDIF-CN_2 2:1 DNTT thin films only signals from the cocrystal and no signals of the pure compounds are visible. Furthermore, the crystallinity of the cocrystal for the equimolar thin films is increasing with higher film thickness and with higher deposition temperature. When comparing the mixing behavior of the two acceptor perylene diimide derivatives with the donor molecule DNTT, the acceptor PDIF-CN_2 with the fluorinated side chain favors the mixing and forms with DNTT a highly defined cocrystal with long-range ordering.

Optical Characterization. Next, we investigate the optical properties of the thin films. In the absorption spectra of both DNTT:$PDIC_8$-CN_2 and DNTT:PDIF-CN_2 systems (Figure 3), excited-state CT peaks are visible at low energy below the HOMO−LUMO transition of the pure compounds. For thin films with $PDIC_8$-CN_2, only a weak CT peak is detected, which is most intense for the equimolar film deposited at room temperature with an onset of a maximum at 1.55 eV (Figure 3b). In contrast, for thin films with PDIF-CN_2 a strong excited-state CT peak with an onset of a maximum at 1.58 eV is visible

https://doi.org/10.1021/acs.jpcc.1c10281
J. Phys. Chem. C 2022, 126, 4188−4198

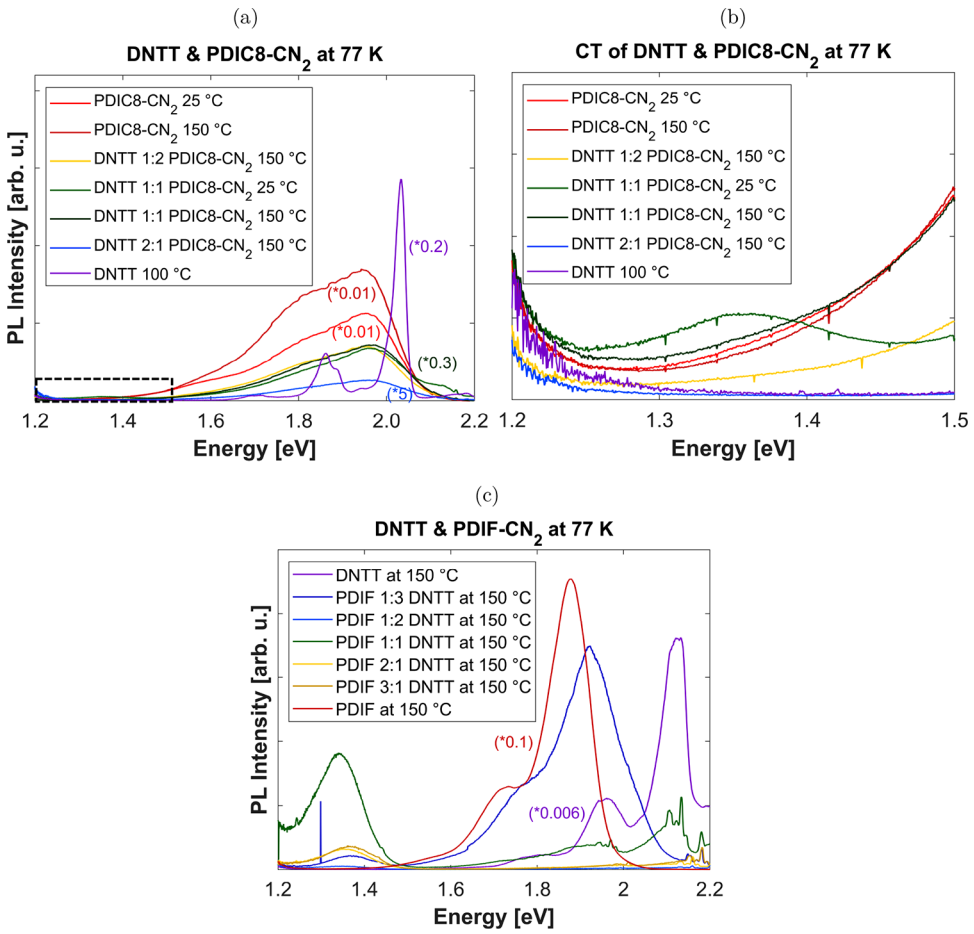

Figure 4. Photoluminescence spectra of (a) DNTT and $PDIC_8$-CN_2 mixed films deposited at 25 and 150 °C, (b) enlarged section of the CT peak (black marked area of part a), and (c) DNTT and PDIF-CN_2 mixed films deposited at 150 °C. The spectra are scaled for clarity, and the signals at about 2.1 and 2.2 eV are background PL signals of the SiO_2 substrate.[55]

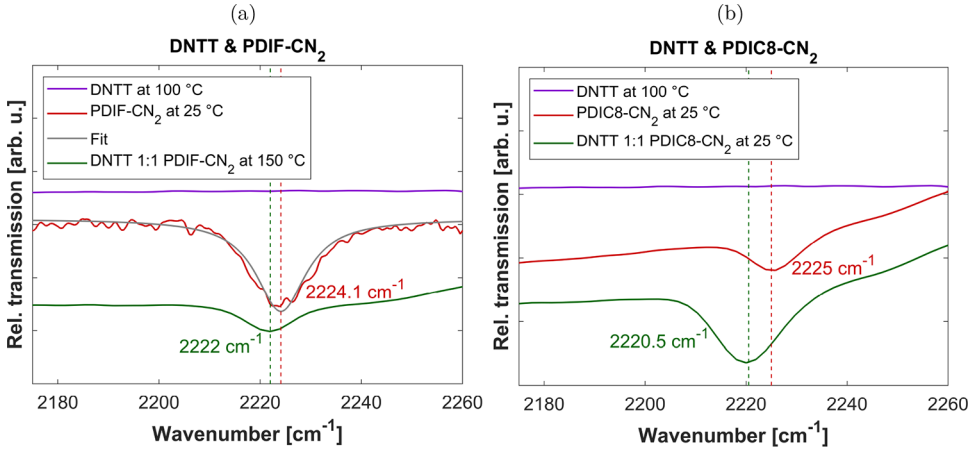

Figure 5. Infrared spectra of (a) DNTT:PDIF-CN_2 equimolar mixed film deposited at 150 °C and (b) DNTT:$PDIC_8$-CN_2 equimolar mixed film deposited at 25 °C.

(Figure 3d). The intensity of the CT peak is increasing with higher deposition temperature. The equimolar 80 nm film of DNTT:PDIF-CN_2 shows two CT states in the absorption spectrum at 1.58 and 1.73 eV.

Figure 4 shows the photoluminescence spectra for DNTT:$PDIC_8$-CN_2 and DNTT:PDIF-CN_2. We find a well-defined CT peak at 1.37 eV of the equimolar $PDIC_8$-CN_2:DNTT mixed film deposited at 25 °C (in Figure 4b). This CT peak is related to the absorption band at 1.55 eV. A shift in PL to lower energy of ~0.2 eV is common for related mixed systems.[30] Features of the pure $PDIC_8$-CN_2 are also visible for the mixed thin films. A strong excited-state CT effect is detected for all DNTT:PDIF-CN_2 mixed thin films (Figure 4c). The CT leads to quenching of the signals of the pure compounds.[56,57] The intensity of the charge transfer peak is

https://doi.org/10.1021/acs.jpcc.1c10281
J. Phys. Chem. C 2022, 126, 4188−4198

largest for the equimolar thin films and decreases with an excess of one of the pure materials.

To study a possible ground state CT, we probe the highly sensitive stretching mode of the nitrile group (CN group) by IR spectroscopy.[58,59] In Figure 5 the infrared spectra for the two PDI:DNTT systems are shown. A shift of 2.1 ± 0.5 cm^{-1} of the CN group is visible for the equimolar DNTT:PDIF-CN_2 mixed film at high deposition temperature. For the equimolar DNTT:$PDIC_8$-CN_2 mixed film at 25 °C the corresponding shift amounts to 4.5 ± 0.4 cm^{-1}. These results indicate a weak partial ground-state charge transfer of 0.08 or 0.17 e^-, respectively, based on an analysis similar to ref 58.

To summarize, the acceptor PDIF-CN_2 with the DNTT donor forms a highly defined cocrystal with long-range order exhibiting a weak ground-state and strong excited-state charge transfer which is increasing with higher substrate temperature and higher film thickness. In contrast, $PDIC_8$-CN_2 forms a cocrystal with DNTT in particular for the substrate at room temperature during growth, showing only weak ES-CT and GS-CT.

Theoretical Characterization. We complement the experimental analysis presented so far with the results of first-principles calculations. We model the DNTT:$PDIC_8$-CN_2 and DNTT:PDIF-CN_2 mixtures as bimolecular clusters *in vacuo*. Both structures are constructed assuming a cofacial arrangement of the two constituting molecules, which remains present also after structural optimization. In the relaxed complexes, as a result of the interactions with the donor, the acceptor molecules show a slight bending of their backbone, as visible in Figure 6.

Inspecting the energy levels of the isolated donor and acceptor molecules (Figure 7), we notice that they form in

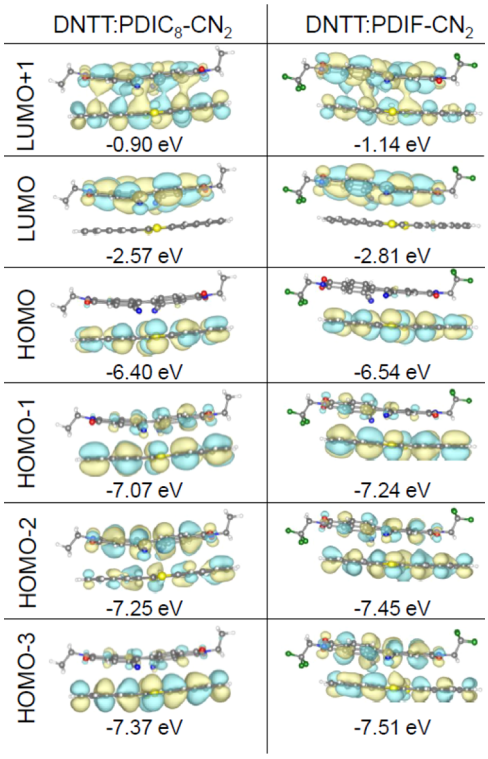

Figure 6. Molecular orbitals of DNTT:$PDIC_8$-CN_2 and DNTT:PDIF-CN_2 accompanied by their respective energy eigenvalues computed from G_0W_0.

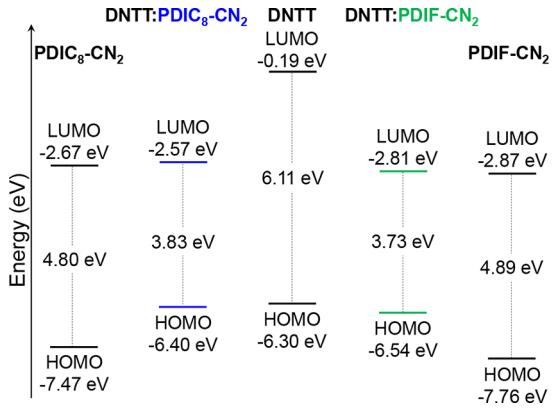

Figure 7. Energy level alignment for both DNTT:$PDIC_8$-CN_2 and DNTT:PDIF-CN_2 complexes computed from G_0W_0 on top of DFT (PBE0 functional).

both cases a type II level alignment, with the lowest-unoccupied molecular orbital (LUMO) of the acceptor lying within the gap of the donor.[60] In DNTT:$PDIC_8$-CN_2 and DNTT:PDIF-CN_2, the highest-occupied molecular orbital (HOMO) is energetically lower than the HOMO of the donor, whereas the LUMO is higher than the LUMO of the acceptor. The energy gap of the complexes is therefore about 0.2 and 0.3 eV larger than the energy difference between the HOMO of DNTT and the LUMO of $PDIC_8$-CN_2 and PDIF-CN_2, respectively. As a result, the HOMO and the LUMO of the complexes are localized on the donor and on the acceptor molecule, respectively (see Figure 6). Hybridization effects appear in lower (higher) occupied (unoccupied) states. This scenario is compatible with the GS-CT, $\delta = 0.11\ e$, obtained for both systems, in agreement with the experimental result for DNTT:PDIF-CN_2 ($\delta = 0.08\ e$).

The calculated absorption spectra for DNTT:$PDIC_8$-CN_2 and DNTT:PDIF-CN_2 are in agreement with the experiments (see Figure 8). The computed absorption peaks are in the same range as the experimental ones although slightly shifted by 0.2 eV, possibly, due to solid-state solvation.[61−63] Differences can be also ascribed to the missing vibronic effects in the calculations. The spectra of the two complexes are very similar. The first excitation (E_1) is found at 1.43 eV in the spectrum of DNTT:$PDIC_8$-CN_2 and at 1.36 eV in the one of DNTT:PDIF-CN_2. In both cases, its oscillator strength is extremely weak, compatible with the negligible overlap between the wave functions associated with the HOMO and the LUMO in the two complexes (see Figure 6): As reported in Table 1, the transition between the frontier orbitals contributes almost entirely to E_1. As a result, the hole and the electron densities are fully segregated on the donor and on the acceptor molecule, respectively (see Figure 9).

The strongest maximum (E_2) is found at ∼2.0 eV and stems from various orbital transitions between occupied orbitals below the HOMO and the LUMO (see Table 1). This feature is reflected in the distribution of the hole and the electron densities: the latter remains localized on the acceptor molecules, while the former is now spread over the whole complex. Analogous behavior pertains also to the third excitation (E_3), which appears as a shoulder above the first peak (see Figure 8). Again, a number of transitions between lower occupied levels and the LUMO characterize its composition in both complexes. Hence, also for E_3, the hole is delocalized on the entire complex while the electron sits

https://doi.org/10.1021/acs.jpcc.1c10281
J. Phys. Chem. C 2022, 126, 4188−4198

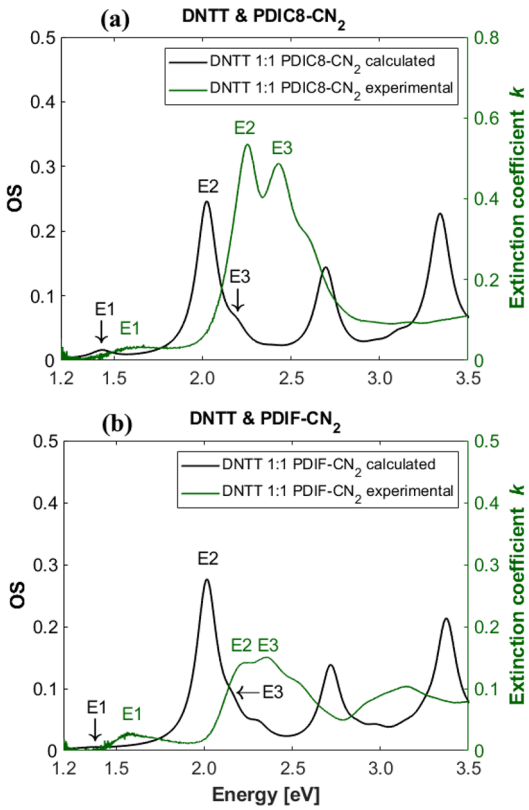

Figure 8. Experimental and computed optical absorption spectra of the complexes (a) DNTT:PDIC$_8$-CN$_2$ and (b) DNTT:PDIF-CN$_2$. The first three excitations are label as E_1, E_2, and E_3. OS stands for oscillator strength.

Table 1. Energies, Oscillator Strength (OS), and Composition in Terms of Single-Quasiparticle Transitions of the First Three Excitations in DNTT:PDIC$_8$-CN$_2$ and DNTT:PDIF-CN$_2$ Complexes[a]

	excitation	energy [eV]	OS	composition
DNTT:PDIC$_8$-CN$_2$	E_1	1.429	0.011	H → L (95%)
	E_2	2.023	0.240	H-1 → L (48%)
				H-3 → L (47%)
	E_3	2.193	0.026	H-1 → L (50%)
				H-2 → L (47%)
DNTT:PDIF-CN$_2$	E_1	1.356	0.001	H → L (95%)
	E_2	2.013	0.266	H-1 → L (42%)
				H-2 → L (31%)
				H-3 → L (24%)
	E_3	2.156	0.035	H-1 → L (50%)
				H-3 → L (34%)
				H-2 → L (11%)

[a]HOMO and LUMO are abbreviated by H and L, respectively.

solely on the acceptor. The fact that all transitions contributing to the first three excitations target only the LUMO can be understood considering the energy separation of more than 1.6 eV between the lowest unoccupied level and the next one (see Figure 6). Conversely, occupied states are energetically much closer to each other. In the calculated spectra, two additional maxima are visible at higher energies, around 2.6 and 3.4 eV. Both peaks, analyzed in detail in the Supporting Information, target higher unoccupied orbitals than the LUMO and correspond to delocalized excitations within the complex.

Discussion. There are different approaches to categorizing the possible CT scenarios. In a rather common one, molecular charge transfer can be divided roughly into three different cases depending on the degree the molecules interact with each other (see Figure 10).[3−5] Systems of organic small molecules, in which the intermolecular energy gap ΔE_{DA} between the HOMO of the donor and the LUMO of the acceptor is similar to the individual energy gaps of the donor (ΔE_D) or acceptor (ΔE_A) molecule, are assigned to the first category (see Figure 10a). In this case, charges are only transferred through molecular excitations (D* or A* states), and no charge transfer effects in the ground state are detectable. Weakly bound acceptor and donor molecules belong to the second category. Here, the individual gaps are larger than the intermolecular energy gap ($\Delta E_{DA} < \Delta E_D$ or ΔE_A, see Figure 10b). This results in weak GS-CT and strong ES-CT effects shown through a peak that can be seen in the absorption or photoluminescence spectra. ES-CT either takes place under direct excitation or via exciton dissociation. Molecular orbitals are only slightly shifted compared to the pure compounds. The last category concerns molecular systems which are strongly bound to each other. The intermolecular energy gap is much smaller than the individual ones ($\Delta E_{DA} \ll \Delta E_D$ or ΔE_A, see Figure 10c). Here, hybridized molecular orbitals are formed with the energy of the CT complex ΔE_{CT}. For these systems, strong ground-state charge transfer effects are detectable by IR spectroscopy.

In the two considered systems (DNTT:PDIC$_8$-CN$_2$ and DNTT:PDIF-CN$_2$), the donor and the two acceptor molecules are weakly bound. This corresponds to the second scenario illustrated above and leads to a partial charge transfer from the donor to the acceptor molecule. This is also supported by experiments and calculations. In the optical spectra of the two investigated mixed cocrystals (see Figure 8), we find a strong excited-state charge transfer band at lower energy in the absorption (∼1.6 eV) and in the emission spectra (∼1.4 eV). Additionally, weak partial GS-CT effects are identified through infrared spectroscopy (see Figure 5), and the amount of partial transferred electron matches with the related calculation.

The interaction between donor and acceptor molecules is affected by molecular packing and structural disorder.[63] Through the design of the acceptor and donor molecules, the positions of the HOMO and LUMO levels can be tuned independently.[59] The physical properties of these compounds are *inter alia* defined by the structure of the resulting donor−acceptor compounds and by the amount of transferred electrons. The required properties, therefore, can be adjusted through the tuned degree of charge transfer.[59]

The localized character of HOMO and LUMO leads to charge transfer effects from the donor to the acceptor as illustrated for the two binary systems in this study. Similar electronic structure and physical properties are also common for other weakly bound acceptor−donor systems.[64−67] A deeper insight into the underlying mechanism is important to understand the fundamental structure−properties relations.[59]

One example for such localized HOMO/LUMO levels and hybridized LUMO+1/HOMO-1 is the cocrystal of the organic small molecules bis(dimethylstyryl)benzene:phenylene bis(bis-(trifluoromethyl)phenyl)acrylonitrile (4M-DSB:CN-TFPA). The large molecular orbital offset between the designed molecules implies the localized HOMO and LUMO level of the donor−acceptor complex. Through the pronounced

https://doi.org/10.1021/acs.jpcc.1c10281
J. Phys. Chem. C 2022, 126, 4188−4198

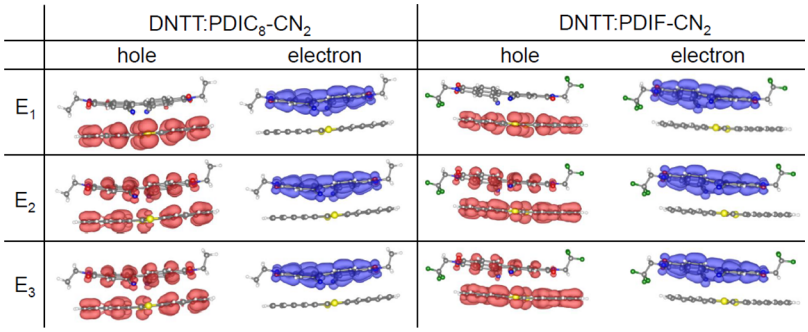

Figure 9. Hole and electron densities calculated for E_1, E_2, and E_3 in the DNTT:PDIC$_8$-CN$_2$ and DNTT:PDIF-CN$_2$ complexes. Isosurfaces plotted with a cutoff of 0.002 Å^{-3}.

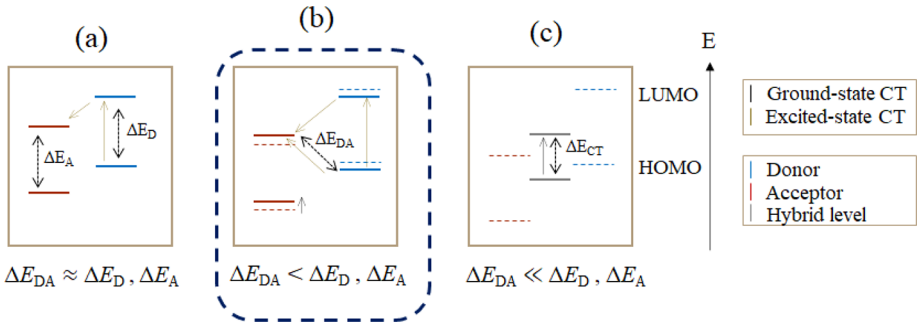

Figure 10. Schematic illustration of possible charge transfer mechanisms for different energy level alignments.

localized character of the frontier molecular orbitals (FMOs), the HOMO−LUMO transition reveals a strong CT character. For this cocrystal also charge transfer effects were investigated.[64] Another example is the system tetracyanoquinodimethane:meso-diphenyltetrathia[22]annulene (TCNQ:DPTTA); in this case the formed cocrystal shows no charge transfer effects.[66] For the system quarterthiophene:tris(pentafluorophenyl)borane (4T:BCF) only excited-state charge transfer effects are detectable clearly related to polaron formation.[67,68] This implies that different charge transfer properties are observed and that GS-CT and ES-CT can occur independently. There are also other organic small molecule combinations (for example, PTCDI-C6:coronene) which show strong charge transfer effects but with slightly different electronic structure of the energy levels. Here, the LUMO and HOMO−1 level are localized.[18] There are different physical properties favored through the electronic structure which are important for such binary systems. Localized FMOs are, for example, an important prerequisite for ambipolar charge transfer.[64−66] These systems favor optical or electrical properties such as high conductivity, ambipolar carrier transport, and tunable luminescence.[18]

To classify our systems (DNTT:PDIC$_8$-CN$_2$ and DNTT:PDIF-CN$_2$) in the possible charge transfer cases, we can compare them with strongly bound acceptor and donor molecules showing a small intermolecular energy gap. For a well-investigated system such as 4T:F4-TCNQ (2,3,5,6-tetrafluoro-7,7,8,8-tetracyanoquinodimethane), the energy levels of the CT complex and its optical properties were calculated and examined.[8,50,69,70] In contrast to our systems, the energy levels of the HOMO LUMO transition are hybridized. 4T:F4-TCNQ shows strong excited-state charge transfer effects in absorption and emission and strong ground-state charge transfer effects visible by IR spectroscopy. These energy level calculations and optical properties are also common for other strongly bound acceptor−donor systems.[71,72] In contrast, they are favored for very efficient electrical doping effects.[8,70]

With the adopted theoretical and experimental methods, our systems can be classified in the second scenario illustrated above belonging to weakly bound molecules where the respective HOMO and LUMO levels are localized.

■ CONCLUSIONS

In summary, a comprehensive study on mixing behavior and charge transfer effects of two donor−acceptor (DNTT:PDI) molecular systems prepared by OMBD has been performed. The two considered acceptor molecules differ in the fluorination of the side chain in the imide position. We investigated the influence of the side chain variation of the acceptor molecules by obtaining a favored mixing behavior and stronger excited-state charge transfer effects for the system DNTT:PDIF-CN$_2$. Charge transfer effects of the mixed thin films increase with raising deposition temperature for the acceptor with fluorinated side chain and decrease for the acceptor with *n*-alkyl side chain. Both systems show a small ground-state CT governed by hybridized HOMO−1 and LUMO+1 levels, while the frontier orbitals are segregated on the donor and acceptor molecule. The calculated optical spectra show similar visible absorption peaks for both systems in agreement with the experimental results. The aforementioned localization for the frontier orbitals leads to a nearly pure charge transfer exciton in the absorption spectra.

With these results, we can make a comparison with other weakly bound donor−acceptor molecules depending on their optical properties and to classify the two PDI:DNTT systems in different charge transfer scenarios.

https://doi.org/10.1021/acs.jpcc.1c10281
J. Phys. Chem. C 2022, 126, 4188−4198

■ ASSOCIATED CONTENT

Supporting Information

The Supporting Information is available free of charge at https://pubs.acs.org/doi/10.1021/acs.jpcc.1c10281.

XRR data of the mixed thin films, additional calculated molecular orbitals, and computed optical spectra (PDF)

■ AUTHOR INFORMATION

Corresponding Author

Nadine Rußegger − *Institut für Angewandte Physik, Universität Tübingen, 72076 Tübingen, Germany;* orcid.org/0000-0003-1746-4170; Email: nadine.russegger@uni-tuebingen.de

Authors

Ana M. Valencia − *Institute of Physics, Carl von Ossietzky Universität Oldenburg, 26129 Oldenburg, Germany; Physics Department and IRIS Adlershof, Humboldt-Universität zu Berlin, 12489 Berlin, Germany*

Lena Merten − *Institut für Angewandte Physik, Universität Tübingen, 72076 Tübingen, Germany*

Matthias Zwadlo − *Institut für Angewandte Physik, Universität Tübingen, 72076 Tübingen, Germany*

Giuliano Duva − *Institut für Angewandte Physik, Universität Tübingen, 72076 Tübingen, Germany; NMI, Naturwissenschaftliches und Medizinisches Institut, 72770 Reutlingen, Germany*

Linus Pithan − *Institut für Angewandte Physik, Universität Tübingen, 72076 Tübingen, Germany*

Alexander Gerlach − *Institut für Angewandte Physik, Universität Tübingen, 72076 Tübingen, Germany; Center for Light−Matter Interaction, Sensors & Analytics Lisa+, Universität Tübingen, 72076 Tübingen, Germany;* orcid.org/0000-0003-1787-1868

Alexander Hinderhofer − *Institut für Angewandte Physik, Universität Tübingen, 72076 Tübingen, Germany; Center for Light−Matter Interaction, Sensors & Analytics Lisa+, Universität Tübingen, 72076 Tübingen, Germany;* orcid.org/0000-0001-8152-6386

Caterina Cocchi − *Institute of Physics, Carl von Ossietzky Universität Oldenburg, 26129 Oldenburg, Germany; Physics Department and IRIS Adlershof, Humboldt-Universität zu Berlin, 12489 Berlin, Germany;* orcid.org/0000-0002-9243-9461

Frank Schreiber − *Institut für Angewandte Physik, Universität Tübingen, 72076 Tübingen, Germany; Center for Light−Matter Interaction, Sensors & Analytics Lisa+, Universität Tübingen, 72076 Tübingen, Germany;* orcid.org/0000-0003-3659-6718

Complete contact information is available at: https://pubs.acs.org/10.1021/acs.jpcc.1c10281

Notes

The authors declare no competing financial interest.

■ ACKNOWLEDGMENTS

The authors gratefully acknowledge the financial support of the German Research Foundation (Deutsche Forschungsgemeinschaft, DFG), Project SCHR 700/20-2. A.M.V. and C.C. acknowledge financial support from the German Research Foundation, Project 182087777 (CRC 951), from the German Federal Ministry of Education and Research (Professorinnenprogramm III) and from the State of Lower Saxony (Professorinnen für Niedersachsen). The computational resources were provided by North-German Supercomputing Alliance (HLRN) through Project bep00076. We acknowledge DESY (Hamburg, Germany), a member of the Helmholtz Association HGF, for the provision of experimental facilities. Parts of this research were performed at PETRA III, and we thank Pallavi Pandit and Stephan Roth for assistance in using beamline P03. The authors thank the European Synchrotron Radiation Facility (ESRF) for providing excellent facilities and the staff from ID03 for their support.

■ REFERENCES

(1) Tang, C. W. Two-layer organic photovoltaic cell. *Appl. Phys. Lett.* **1986**, *48*, 183−185.

(2) Brédas, J.-L.; Norton, J. E.; Cornil, J.; Coropceanu, V. Molecular Understanding of Organic Solar Cells: The Challenges. *Acc. Chem. Res.* **2009**, *42*, 1691−1699.

(3) Vandewal, K. Interfacial Charge Transfer States in Condensed Phase Systems. *Annu. Rev. Phys. Chem.* **2016**, *67*, 113−133.

(4) Vandewal, K.; Albrecht, S.; Hoke, E. T.; Graham, K. R.; Widmer, J.; Douglas, J. D.; Schubert, M.; Mateker, W. R.; Bloking, J. T.; Burkhard, G. F.; et al. Efficient Charge Generation by Relaxed Charge-Transfer States at Organic Interfaces. *Nat. Mater.* **2014**, *13*, 63−68.

(5) Belova, V.; Beyer, P.; Meister, E.; Linderl, T.; Halbich, M.-U.; Gerhard, M.; Schmidt, S.; Zechel, T.; Meisel, T.; Generalov, A. V.; et al. Evidence for Anisotropic Electronic Coupling of Charge Transfer States in Weakly Interacting Organic Semiconductor Mixtures. *J. Am. Chem. Soc.* **2017**, *139*, 8474−8486.

(6) Hinderhofer, A.; Schreiber, F. Organic-Organic Heterostructures: Concepts and Applications. *ChemPhysChem* **2012**, *13*, 628−643.

(7) Ruderer, M. A.; Müller-Buschbaum, P. Morphology of polymer-based bulk heterojunction films for organic photovoltaics. *Soft Matter* **2011**, *7*, 5482−5493.

(8) Méndez, H.; Heimel, G.; Winkler, S.; Frisch, J.; Opitz, A.; Sauer, K.; Wegner, B.; Oehzelt, M.; Röthel, C.; Duhm, S.; et al. Charge-Transfer Crystallites as Molecular Electrical Dopants. *Nat. Commun.* **2015**, *6*, 8560.

(9) Broch, K.; Dieterle, J.; Branchi, F.; Hestand, N. J.; Olivier, Y.; Tamura, H.; Cruz, C.; Nichols, V. M.; Hinderhofer, A.; Beljonne, D.; et al. Robust singlet fission in pentacene thin films with tuned charge transfer interactions. *Nat. Commun.* **2018**, *9*, 954.

(10) Schwarze, M.; Schellhammer, K. S.; Ortstein, K.; Benduhn, J.; Gaul, C.; Hinderhofer, A.; Toro, L. P.; Scholz, R.; Kublitski, J.; Roland, S.; et al. Impact of molecular quadrupole moments on the energy levels at organic heterojunctions. *Nat. Commun.* **2019**, *10*, 2466.

(11) Liscio, F.; Milita, S.; Albonetti, C.; D'Angelo, P.; Guagliardi, A.; Masciocchi, N.; Della Valle, R. G.; Venuti, E.; Brillante, A.; Biscarini, F. Structure and Morphology of PDI8-CN2 for n-Type Thin-Film Transistors. *Adv. Funct. Mater.* **2012**, *22*, 943−953.

(12) Sun, Y.; Liu, Y.; Zhu, D. Advances in organic field-effect transistors. *J. Mater. Chem.* **2005**, *15*, 53−65.

(13) Rahimi, R.; Narang, V.; Korakakis, D. Optical and Morphological Studies of Thermally Evaporated PTCDI-C8 Thin Films for Organic Solar Cell Applications. *Int. J. Photoenergy* **2013**, *2013*, 1−7.

(14) Sugie, A.; Han, W.; Shioya, N.; Hasegawa, T.; Yoshida, H. Structure-Dependent Electron Affinities of Perylene Diimide-Based Acceptors. *J. Phys. Chem. C* **2020**, *124*, 9765−9773.

(15) Jones, B. A.; Facchetti, A.; Wasielewski, M. R.; Marks, T. J. Tuning Orbital Energetics in Arylene Diimide Semiconductors. Materials Design for Ambient Stability of n-Type Charge Transport. *J. Am. Chem. Soc.* **2007**, *129*, 15259−15278.

(16) Jung, B. J.; Tremblay, N. J.; Yeh, M.-L.; Katz, H. E. Molecular Design and Synthetic Approaches to Electron-Transporting Organic Transistor Semiconductors. *Chem. Mater.* **2011**, *23*, 568−582.
(17) Pron, A.; Gawrys, P.; Zagorska, M.; Djurado, D.; Demadrille, R. Electroactive materials for organic electronics: preparation strategies, structural aspects and characterization techniques. *Chem. Soc. Rev.* **2010**, *39*, 2577−2632.
(18) Wang, C.; Wang, J.; Wu, N.; Xu, M.; Yang, X.; Lu, Y.; Zang, L. Donor−acceptor single cocrystal of coronene and perylene diimide: molecular self-assembly and charge-transfer photoluminescence. *RSC Adv.* **2017**, *7*, 2382−2387.
(19) Fan, H.; Shi, W.; Yu, X.; Yu, J. High performance nitrogen dioxide sensor based on organic field-effect transistor utilizing ultrathin CuPc/PTCDI-C8 heterojunction. *Synth. Met.* **2016**, *211*, 161−166.
(20) Aghamohammadi, M.; Fernández, A.; Schmidt, M.; Pérez-Rodríguez, A.; Goñi, A. R.; Fraxedas, J.; Sauthier, G.; Paradinas, M.; Ocal, C.; Barrena, E. Influence of the Relative Molecular Orientation on Interfacial Charge-Transfer Excitons at Donor/Acceptor Nanoscale Heterojunctions. *J. Phys. Chem. C* **2014**, *118*, 14833−14839.
(21) Yagi, H.; Miyazaki, T.; Tokumoto, Y.; Aoki, Y.; Zenki, M.; Zaima, T.; Okita, S.; Yamamoto, T.; Miyazaki, E.; Takimiya, K.; et al. Ultraviolet photoelectron spectra of 2,7-diphenyl[1]benzothieno[3,2-b][1]benzothiophene and dinaphtho[2,3-b:2′,3′-f]thieno[3,2-b]-thiophene. *Chem. Phys. Lett.* **2013**, *563*, 55−57.
(22) Kuribara, K.; Wang, H.; Uchiyama, N.; Fukuda, K.; Yokota, T.; Zschieschang, U.; Jaye, C.; Fischer, D.; Klauk, H.; Yamamoto, T.; et al. Organic transistors with high thermal stability for medical applications. *Nat. Commun.* **2012**, *3*, 723.
(23) Zschieschang, U.; Ante, F.; Kälblein, D.; Yamamoto, T.; Takimiya, K.; Kuwabara, H.; Ikeda, M.; Sekitani, T.; Someya, T.; Blochwitz-Nimoth, J.; et al. Dinaphtho[2,3-b:2′,3′-f]thieno[3,2-b]-thiophene (DNTT) thin-film transistors with improved performance and stability. *Org. Electron.* **2011**, *12*, 1370−1375.
(24) Belova, V.; Hinderhofer, A.; Zeiser, C.; Storzer, T.; Rozbořil, J.; Hagenlocher, J.; Novák, J.; Gerlach, A.; Scholz, R.; Schreiber, F. Structure-Dependent Charge Transfer in Molecular Perylene-Based Donor/Acceptor Systems and Role of Side Chains. *J. Phys. Chem. C* **2020**, *124*, 11639−11651.
(25) Schreiber, F. Organic molecular beam deposition: Growth studies beyond the first monolayer. *phys. stat. sol. (a)* **2004**, *201*, 1037−1054.
(26) Forrest, S. R. Ultrathin organic films grown by organic molecular beam deposition and related techniques. *Chem. Rev.* **1997**, *97*, 1793−1896.
(27) Björck, M.; Andersson, G. GenX: an extensible X-ray reflectivity refinement program utilizing differential evolution. *J. Appl. Crystallogr.* **2007**, *40*, 1174−1178.
(28) Parratt, L. G. Surface Studies of Solids by Total Reflection of X-Rays. *Phys. Rev.* **1954**, *95*, 359−369.
(29) Buffet, A.; Rothkirch, A.; Döhrmann, R.; Körstgens, V.; Kashem, M. M. A.; Perlich, J.; Herzog, G.; Schwartzkopf, M.; Gehrke, R.; Müller-Buschbaum, P.; et al. P03, the microfocus and nanofocus X-ray scattering (MiNaXS) beamline of the PETRA III storage ring: the microfocus endstation. *J. Synchr. Radiat.* **2012**, *19*, 647−653.
(30) Anger, F.; Ossó, J. O.; Heinemeyer, U.; Broch, K.; Scholz, R.; Gerlach, A.; Schreiber, F. Photoluminescence spectroscopy of pure pentacene, perfluoropentacene, and mixed thin films. *J. Chem. Phys.* **2012**, *136*, No. 054701.
(31) Buzio, R.; Gerbi, A.; Marrè, D.; Barra, M.; Cassinese, A. Electron injection barrier and energy-level alignment at the Au/PDI8-CN2 interface via current−voltage measurements and ballistic emission microscopy. *Org. Electron.* **2015**, *18*, 44−52.
(32) Hohenberg, P.; Kohn, W. Inhomogeneous Electron Gas. *Phys. Rev.* **1964**, *136*, B864−B871.
(33) Kohn, W.; Sham, L. J. Self-Consistent Equations Including Exchange and Correlation Effects. *Phys. Rev.* **1965**, *140*, A1133−A1138.
(34) Hedin, L. New Method for Calculating the One-Particle Green's Function with Application to the Electron-Gas Problem. *Phys. Rev.* **1965**, *139*, A796−A823.
(35) Hybertsen, M. S.; Louie, S. G. Electron Correlation in Semiconductors and Insulators: Band Gaps and Quasiparticle Energies. *Phys. Rev. B* **1986**, *34*, 5390.
(36) Hanke, W.; Sham, L. J. Many-Particle Effects in the Optical Spectrum of a Semiconductor. *Phys. Rev. B* **1980**, *21*, 4656−4673.
(37) Blum, V.; Gehrke, R.; Hanke, F.; Havu, P.; Havu, V.; Ren, X.; Reuter, K.; Scheffler, M. Ab Initio Molecular Simulations with Numeric Atom-Centered Orbitals. *Comput. Phys. Commun.* **2009**, *180*, 2175−2196.
(38) Havu, V.; Blum, V.; Havu, P.; Scheffler, M. Efficient O(N) Integration for All-Electron Electronic Structure Calculation Using Numeric Basis Functions. *J. Comput. Phys.* **2009**, *228*, 8367−8379.
(39) Perdew, J. P.; Burke, K.; Ernzerhof, M. Generalized Gradient Approximation Made Simple. *Phys. Rev. Lett.* **1996**, *77*, 3865−3868.
(40) Tkatchenko, A.; Scheffler, M. Accurate Molecular Van Der Waals Interactions from Ground-State Electron Density and Free-Atom Reference Data. *Phys. Rev. Lett.* **2009**, *102*, No. 073005.
(41) Hirshfeld, F. L. Bonded-Atom Fragments for Describing Molecular Charge Densities. *Theor. Chim. Acta* **1977**, *44*, 129−138.
(42) Bruneval, F.; Rangel, T.; Hamed, S. M.; Shao, M.; Yang, C.; Neaton, J. B. MOLGW 1: Many-Body Perturbation Theory Software for Atoms, Molecules, and Clusters. *Comput. Phys. Commun.* **2016**, *208*, 149−161.
(43) Bruneval, F. Ionization Energy of Atoms Obtained from GW Self-Energy or from Random Phase Approximation Total Energies. *J. Chem. Phys.* **2012**, *136*, 194107.
(44) Weigend, F.; Köhn, A.; Hättig, C. Efficient Use of the Correlation Consistent Basis Sets in Resolution of the Identity MP2 Calculations. *J. Chem. Phys.* **2002**, *116*, 3175−3183.
(45) Adamo, C.; Barone, V. Toward Reliable Density Functional Methods Without Adjustable Parameters: The PBE0Model. *J. Chem. Phys.* **1999**, *110*, 6158−6170.
(46) Faber, C.; Boulanger, P.; Duchemin, I.; Attaccalite, C.; Blase, X. Many-Body Green's Function GW and Bethe-Salpeter Study of the Optical Excitations in a Paradigmatic Model Dipeptide. *J. Chem. Phys.* **2013**, *139*, 194308.
(47) Bruneval, F.; Marques, M. A. L. Benchmarking the Starting Points of the GW Approximation for Molecules. *J. Chem. Theory. Comput.* **2013**, *9*, 324−329.
(48) Rangel, T.; Hamed, S. M.; Bruneval, F.; Neaton, J. B. An assessment of low-lying excitation energies and triplet instabilities of organic molecules with an ab initio Bethe-Salpeter equation approach and the Tamm-Dancoff approximation. *J. Chem. Phys.* **2017**, *146*, 194108.
(49) Cocchi, C.; Prezzi, D.; Ruini, A.; Caldas, M. J.; Molinari, E. Optical properties and charge-transfer excitations in edge-functionalized all-graphene nanojunctions. *J. Phys. Chem. Lett.* **2011**, *2*, 1315−1319.
(50) Valencia, A. M.; Cocchi, C. Electronic and Optical Properties of Oligothiophene-F4TCNQ Charge-Transfer Complexes: The Role of the Donor Conjugation Length. *J. Phys. Chem. C* **2019**, *123*, 9617−9623.
(51) Chen, W.; Nikiforov, M. P.; Darling, S. B. Morphology characterization in organic and hybrid solar cells. *Energy Environ. Sci.* **2012**, *5*, 8045−8074.
(52) Müller-Buschbaum, P. The Active Layer Morphology of Organic Solar Cells Probed with Grazing Incidence Scattering Techniques. *Adv. Mater.* **2014**, *26*, 7692−7709.
(53) Rivnay, J.; Mannsfeld, S. C. B.; Miller, C. E.; Salleo, A.; Toney, M. F. Quantitative Determination of Organic Semiconductor Microstructure from the Molecular to Device Scale. *Chem. Rev.* **2012**, *112*, 5488−5519.
(54) Belova, V.; Wagner, B.; Reisz, B.; Zeiser, C.; Duva, G.; Rozbořil, J.; Novák, J.; Gerlach, A.; Hinderhofer, A.; Schreiber, F. Real-Time Structural and Optical Study of Growth and Packing Behavior of

https://doi.org/10.1021/acs.jpcc.1c10281
J. Phys. Chem. C 2022, 126, 4188−4198

Perylene Diimide Derivative Thin Films: Influence of Side-Chain Modification. *J. Phys. Chem. C* **2018**, *122*, 8589−8601.
(55) Hummel, R. E.; Chang, S.-S. Novel technique for preparing porous silicon. *Appl. Phys. Lett.* **1992**, *61*, 1965−1967.
(56) Gierschner, J.; Mack, H.-G.; Oelkrug, D.; Waldner, I.; Rau, H. Modeling of the Optical Properties of Cofacial Chromophore Pairs: Stilbenophane. *J. Phys. Chem. A* **2004**, *108*, 257−263.
(57) Gierschner, J.; Ehni, M.; Egelhaaf, H.-J.; Medina, B. M.; Beljonne, D.; Benmansour, H.; Bazan, G. C. Solid-state optical properties of linear polyconjugated molecules: π-stack contra herringbone. *J. Chem. Phys.* **2005**, *123*, 144914.
(58) Chappell, J.; Bloch, A.; Bryden, W.; Maxfield, M.; Poehler, T.; Cowan, D. Degree of charge transfer in organic conductors by infrared absorption spectroscopy. *J. Am. Chem. Soc.* **1981**, *103*, 2442−2443.
(59) Jiang, H.; Hu, P.; Ye, J.; Zhang, K. K.; Long, Y.; Hu, W.; Kloc, C. Tuning of the degree of charge transfer and the electronic properties in organic binary compounds by crystal engineering: a perspective. *J. Mater. Chem. C* **2018**, *6*, 1884−1902.
(60) Oehzelt, M.; Akaike, K.; Koch, N.; Heimel, G. Energy-level alignment at organic heterointerfaces. *Sci. Adv.* **2015**, *1*, No. e1501127.
(61) Madigan, C. F.; Bulović, V. Solid State Solvation in Amorphous Organic Thin Films. *Phys. Rev. Lett.* **2003**, *91*, 247403.
(62) Imbrasas, P.; Lygaitis, R.; Kleine, P.; Scholz, R.; Hänisch, C.; Buchholtz, S.; Ortstein, K.; Talnack, F.; Mannsfeld, S. C. B.; Lenk, S.; et al. Dimers or Solid-State Solvation? Intermolecular Effects of Multiple Donor−Acceptor Thermally Activated Delayed Fluorescence Emitter Determining Organic Light-Emitting Diode Performance. *Adv. Optical Mater.* **2021**, *9*, 2002153.
(63) Guerrini, M.; Valencia, A. M.; Cocchi, C. Long-Range Order Promotes Charge-Transfer Excitations in Donor/Acceptor Co-Crystals. *J. Phys. Chem. C* **2021**, *125*, 20821−20830.
(64) Park, S. K.; Varghese, S.; Kim, J. H.; Yoon, S.-J.; Kwon, O. K.; An, B.-K.; Gierschner, J.; Park, S. Y. Tailor-Made Highly Luminescent and Ambipolar Transporting Organic Mixed Stacked Charge-Transfer Crystals: An Isometric Donor−Acceptor Approach. *J. Am. Chem. Soc.* **2013**, *135*, 4757−4764.
(65) Geng, H.; Zhu, L.; Yi, Y.; Zhu, D.; Shuai, Z. Superexchange Induced Charge Transport in Organic Donor−Acceptor Cocrystals and Copolymers: A Theoretical Perspective. *Chem. Mater.* **2019**, *31*, 6424−6434.
(66) Zhang, J.; Geng, H.; Virk, T. S.; Zhao, Y.; Tan, J.; an Di, C.; Xu, W.; Singh, K.; Hu, W.; Shuai, Z.; et al. Sulfur-Bridged Annulene-TCNQ Co-Crystal: A Self-Assembled "Molecular Level Heterojunction" with Air Stable Ambipolar Charge Transport Behavior. *Adv. Mater.* **2012**, *24*, 2603−2607.
(67) Schier, R.; Valencia, A. M.; Cocchi, C. Microscopic Insight into the Electronic Structure of BCF-Doped Oligothiophenes from Ab Initio Many-Body Theory. *J. Phys. Chem. C* **2020**, *124*, 14363−14370.
(68) Mansour, A. E.; Lungwitz, D.; Schultz, T.; Arvind, M.; Valencia, A. M.; Cocchi, C.; Opitz, A.; Neher, D.; Koch, N. The optical signatures of molecular-doping induced polarons in poly(3-hexylthiophene-2,5-diyl): individual polymer chains versus aggregates. *J. Mater. Chem. C* **2020**, *8*, 2870−2879.
(69) Valencia, A. M.; Guerrini, M.; Cocchi, C. Ab Initio Modelling of Local Interfaces in Doped Organic Semiconductors. *Phys. Chem. Chem. Phys.* **2020**, *22*, 3527−3538.
(70) Zhu, L.; Kim, E.-G.; Yi, Y.; Brédas, J.-L. Charge Transfer in Molecular Complexes with 2,3,5,6-Tetrafluoro-7,7,8,8-tetracyanoquinodimethane (F4-TCNQ): A Density Functional Theory Study. *Chem. Mater.* **2011**, *23*, 5149−5159.
(71) Mahns, B.; Kataeva, O.; Islamov, D.; Hampel, S.; Steckel, F.; Hess, C.; Knupfer, M.; Büchner, B.; Himcinschi, C.; Hahn, T.; et al. Crystal Growth, Structure, and Transport Properties of the Charge-Transfer Salt Picene/2,3,5,6-Tetrafluoro-7,7,8,8-tetracyanoquinodimethane. *Cryst. Growth Des.* **2014**, *14*, 1338−1346.
(72) Salzmann, I.; Heimel, G.; Duhm, S.; Oehzelt, M.; Pingel, P.; George, B. M.; Schnegg, A.; Lips, K.; Blum, R.-P.; Vollmer, A.; et al. Intermolecular Hybridization Governs Molecular Electrical Doping. *Phys. Rev. Lett.* **2012**, *108*, No. 035502.

https://doi.org/10.1021/acs.jpcc.1c10281
J. Phys. Chem. C 2022, 126, 4188−4198